Structure of a Switchable Subtilisin Complexed with a Substrate and with the Activator Azide[†]

Travis Gallagher,*,[‡,§] Biao Ruan,[‡,||] Mariya London,[‡,||] Molly A. Bryan,[‡,||] and Philip N. Bryan[‡,⊥]

[‡]*Center for Advanced Research in Biotechnology, 9600 Gudelsky Drive, Rockville, Maryland 20850,* [§]*National Institute of Standards and Technology, Gaithersburg, Maryland 20899,* [||]*Potomac Affinity Proteins, LLC, Gaithersburg, Maryland 20878, and* [⊥]*University of Maryland Biotechnology Institute, Baltimore, Maryland 21202*

ABSTRACT: An engineered variant of the protease subtilisin from *Bacillus amyloliquefaciens*, in which the D32A mutation renders the enzyme's activity dependent on the presence of certain small anions such as fluoride or azide, has been produced. This modified enzyme has applications as an azide or fluoride-triggered expression−purification tool. We report activity measurements showing that the enzyme is activated more than 3000-fold by azide and describe the 1.8 Å resolution structure of an inactive form (by replacing the catalytic nucleophile Ser 221 with alanine) of the protease, in complex with azide and with a substrate that spans the active site. Both enzyme and substrate have been engineered to increase their stability and the affinity of their interaction. The substrate is based on a stabilized subtilisin prodomain, extended across the active site by the addition of four residues at its C-terminus. In the crystal structure, the substrate is well-ordered across the active site, and the azide anion is observed bound adjacent to Ala 32. The structures of the substrate complex in three different crystals (anion-free, fluoride-soaked, and azide-soaked) are compared. These structures provide extensive information for understanding subtilisin's substrate binding and catalytic mechanism, and for the development of biotechnology tools based on anion-activated proteolysis. The mechanism of anion-dependent proteolysis appears to be a slight modification of the accepted charge-relay mechanism for serine proteases.

The secreted serine protease subtilisin BPN′ from *Bacillus amyloliquefaciens* is active against a broad range of substrate sequences, appropriate for digestion of extracellular proteins (*1−3*). Like all secreted proteases, subtilisin is initially synthesized as a proenzyme (*4*). Prosubtilisin is autoprocessed to create a transient complex of the 77-amino acid N-terminal prodomain and the 275-amino acid mature enzyme (*5, 6*). Substrate preferences are typified by the cleavage site of prosubtilisin, which is the substrate in the enzyme's autocatalytic maturation process. The cleavage site has the sequence AHAY.AQSV, with the AHAY portion becoming the C-terminus of the 77-residue prodomain and the AQSV portion becoming the N-terminus of the mature enzyme (*7*). Extensive structural and enzymatic data have shown that most substrate contacts are made with the first four residues on the acyl side of the scissile bond, which are denoted P1−P4, numbering from the scissile bond toward the N-terminus of the substrate (*8*). The most effective substrates include a large uncharged residue at P1, Ser or Ala at P2, and a hydrophobe at P4 (*9, 10*).

Previously, we have engineered subtilisin into a specific, processing protease and coengineered the prodomain into an optimized recognition sequence. This involved four steps: (1) engineering of highly stable and refoldable subtilisin (*11, 12*), (2) modifications of binding pockets resulting in a strong preference for sequences of the form P4−P1 = YRAL (*13−17*), (3) selection of an independently stable prodomain with high affinity for subtilisin (*18, 19*), and (4) engineering a tunable active site by means of a D32A[1] mutation which renders activity dependent on the presence of certain small anions such as fluoride and azide (*20−22*). The resulting switchable subtilisin, whose activity against cognate sequences (e.g., YRAL-) can be accelerated more than 3000-fold by 100 mM azide, is denoted S189.

The ability to modulate the rate of the cleavage reaction with anion concentration creates a processing system with a virtual on−off switch. Switchable proteases are useful biotechnologically as well as in studies of mechanism. The anion-switchable subtilisin has been used to develop a one-step affinity chromatography system for the purification of recombinant proteins. The purification system comprises a target protein fused to the C-terminus of an engineered prodomain and an immobilized subtilisin that is virtually inactive in the absence of a triggering anion. The ability to isolate the binding and cleavage steps with a triggering mechanism allows subtilisin to be used as both the affinity ligand and processing enzyme for affinity purification and processing of proteins fused to the prodomain (*21*). The

---

*To whom correspondence should be addressed. Telephone: (240) 314-6204. Fax: (240) 314-6225. E-mail: gallaghe@umbi.umd.edu.

[1]A shorthand for denoting amino acid substitutions employs the single-letter amino acid code as follows: N218S denotes the change of asparagine 218 to serine, and Δ75−83 denotes the deletion of residues 75−83 from the amino acid sequence. Abbreviations: DMSO, dimethyl sulfoxide; DTT, dithiothreitol; EDTA, ethylenediaminetetraacetic acid; HEPES, 4-(2-hydroxyethyl)-1-piperazineethanesulfonic acid; PAGE, polyacrylamide gel electrophoresis; PEG, polyethylene glycol; RCSB, Research Collaboratory for Structural Bioinformatics; SDS, sodium dodecyl sulfate.

commercial version of this purification system is the Profinity eXact Purification System (Bio-Rad Laboratories), and similar components are used for measurement of azide-dependent cleavage rates in this paper.

Here we report anion-dependent cleavage kinetics for subtilisin S189 and describe the 1.8 Å resolution crystal structure of complexes of an inactive (S221A) form of S189 and a prodomain substrate. The crystallized prodomain construct, called pG16, includes a four-residue C-terminal tail with a SATS sequence and thus provides structural information about substrate interactions spanning the active site. Although S189, like wild-type subtilisin, has Ser as the catalytic nucleophile at residue 221, these crystal structures have Ala 221 to prevent cleavage of the substrate. We report the structure of the subtilisin−substrate complex without triggering anion, with fluoride, and with the activator azide. The resulting structures and corresponding kinetic analysis provide detailed views of protease−substrate interactions and insight into the mechanisms of catalysis and activation by anions.

METHODS

Definition of Mutants. (*i*) *Subtilisin.* S189 is our basic processing subtilisin whose engineering has been described earlier. S189 denotes subtilisin from *B. amyloliquefaciens* with the following mutations: Q2K, S3C, P5S, S9A, I31L, D32A, K43N, M50F, A73L, Δ75−83, Y104A, G128S, E156S, G166S, G169A, S188P, Q206C, N212G, Y217L, N218S, T254A, and Q271E (*21*, *23−26*). We have constructed two new variants of S189 for this study. The first variant (denoted pS164) is the S221A mutant of S189. As noted above, mutation of the active site serine inactivates the enzyme and allows structural characterization of substrate interactions that span the active site. The second variant, denoted pS169, is the A1C mutant of S189. This mutation does not change the catalytic properties of the enzyme but allows the introduction of a fluorescent group at its N-terminus. The site specific label is useful for kinetic analysis as described below.

(*ii*) *Prodomain.* pG60 is a stabilized version of the prodomain used in previous studies (*19*). pG60 denotes the prodomain from *B. amyloliquefaciens* with the following mutations: substitution of amino acids 17−21 (TMSTM) with GFK and substitutions A23C, K27E, V37L, Q40C, H72K, A74Y, H75R, and Y77L. pG60 is independently stable and binds to subtilisin with ~100-fold higher affinity than the wild-type prodomain. We have constructed two new variants of pG60 for this study. The first variant, denoted pG16, constructed for the crystallographic studies, has four amino acids added to its C-terminus: S78, A79, T80, and S81. The second variant, denoted pG12, constructed for the kinetic measurements, is pG16 followed by the 56-amino acid B_1 domain of protein G (G_B) (*27*, *28*), whose tryptophan fluorescence facilitates monitoring of proteolytic release (see below).

Expression and Purification. Subtilisin variants pS164 and pS169 were expressed in *Escherichia coli* as described for similar variants in ref *29*, except that the peptide affinity purification column used an immobilized peptide of the sequence LFRAL rather than ALAL. Prodomain variants pG12 and pG16 were expressed in *E. coli* as described for similar variants in ref *21*, except they were released from the S189 subtilisin column by elution in 0.1 M H_3PO_4 (pH 2.1) rather than by anion-triggered cleavage. Purity was assessed by SDS−PAGE and estimated to be >95%.
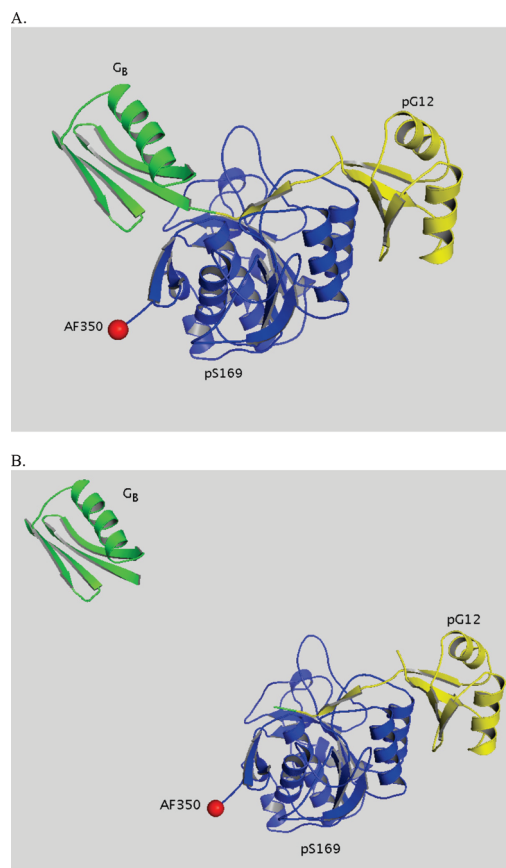

FIGURE 1: (A) Cartoon representation of the pG12 fusion protein (green and yellow) in complex with pS169 subtilisin (blue). The position of the fluorescent reporter is colored red on the pS169 N-terminus. (B) Cartoon representation of G_B and the pG12−pS169 complex after cleavage.

Measurement of Activity of Subtilisin pS169 as a Function of Anion. The N-terminal amino acid is the only free cysteine in pS169 and enables specific labeling with maleimide reagents. pS169 for kinetic measurements was labeled with Alexafluor 350 maleimide. *E. coli* extract containing 20 mM DTT was washed over a 1 mL LFRAL column to allow affinity binding of pS169. The column was washed with 20 mL of 10 mM HEPES (pH 6.8), 100 mM NaCl, and 1 mM EDTA (HNE). A 1.4 mL volume of a 10 mM solution of Alexafluor 350 maleimide in HNE and 20% DMSO was injected on the column and incubated for 2 h at 22 °C. Excess label was then washed away in HNE. The labeled protein was eluted in 10 mM NH_4OH and immediately neutralized with $^1/_{10}$ volume of 1 M potassium phosphate (pH 7.2).

Attached to the N-terminus of pS169, Alexafluor 350 becomes a fluorescent reporter group with an absorption maximum at 350 nm and an emission maximum at 450 nm. The substrate for kinetic measurements was pG12 (Figure 1). pG12 forms a highly stable complex with labeled pS169. In this complex, the single tryptophan of G_B can be excited at 300 nm so that some energy is transferred to Alexafluor 350, the emission of which at 450 nm can then be monitored. Enzymatic cleavage releases G_B from the complex and results in a decrease in the level of energy transfer, enabling time-dependent quantitation of proteolysis. The total fluorescence signal at 450 nm decreases by ~8% upon complete cleavage of the substrate complex into the product complex and G_B.
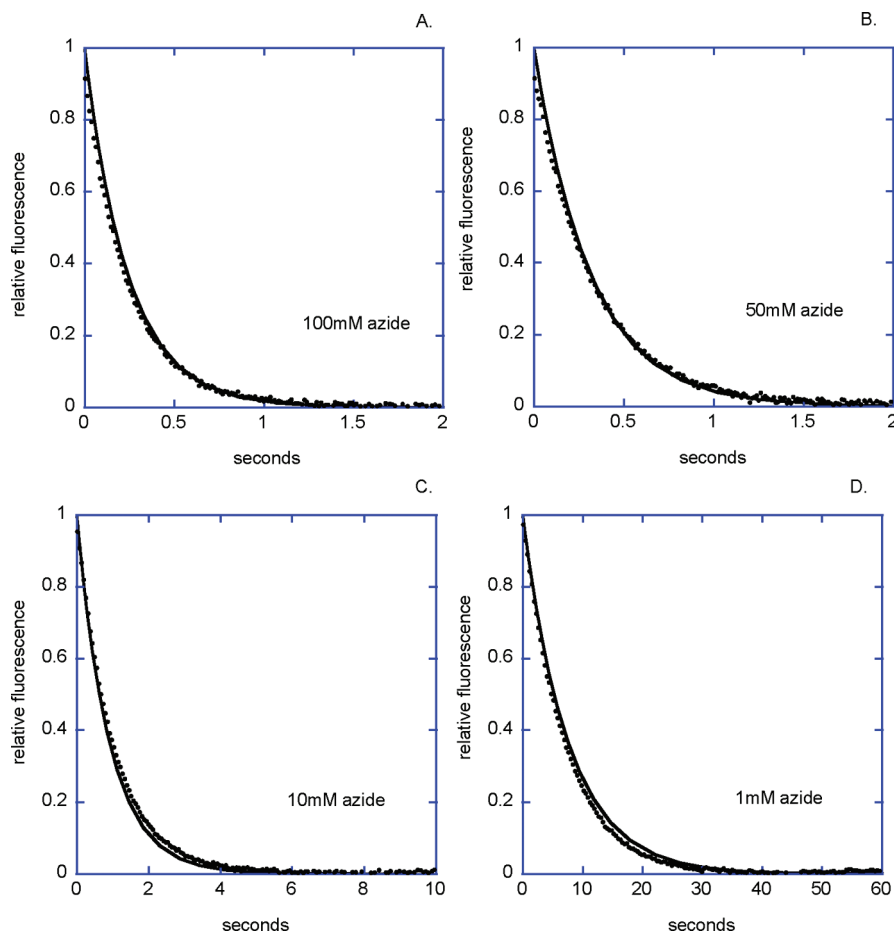
FIGURE 2: Kinetics of azide-dependent proteolysis of substrate pG12 by Sbt169. The concentration of the enzyme−substrate complex was 1 μM in 0.1 M KPO$_4$ (pH 7.2, 22 °C) and (A) 100 mM azide, (B) 50 mM azide, (C) 10 mM azide, and (D) 1 mM azide. The release of G$_B$ is followed by fluorescence for each azide concentration (●). Solid lines are fits to Scheme 1 obtained with KinTek Global Explorer. Similar measurements for formate, cyanate, fluoride, and chloride resulted in the values in Table 1.

Reaction rates were measured using a KinTek stopped-flow model SF2001 instrument (excitation λ = 300 nm, and emission with a 450 nm cutoff filter). Stock solutions of Alexafluor-labeled pS169 at a concentration of 100 μM and pG12 at a concentration of 350 μM, both in 100 mM KP$_i$ (pH 7.2), were prepared and equilibrated at 22 °C. Immediately prior to stop-flow mixing, enzyme and substrate were combined and diluted each to a concentration of 2 μM, in 100 mM KP$_i$ (pH 7.2), and placed in syringe A of the SF2001 instrument. Solutions of triggering anion in the same buffer were placed in syringe B. Fluorescence data were collected after 1:1 mixing of the two solutions. The final anion concentration was varied from 0 to 100 mM for azide, from 0 to 500 mM for cyanate and formate, and from 0 to 1 M for fluoride and chloride. The final concentration of the protein complex was fixed at 1 μM. The rates of azide triggering were also determined in 100 mM KP$_i$ (pH 7.2) with 250 and 500 mM KCl. The rate of G$_B$ release was followed by the decrease in fluorescence at 450 nm. At least 10 kinetic traces were collected for each concentration of anion. Kinetic data were fit using KinTek Global Explorer obtained from KinTek Corp. (www.kintek-corp.com).

Crystallization and Structure Analysis. The s164−pG16 complex was crystallized from 15% (v/v) PEG 8000, 0.2 M zinc acetate, and 0.1 M sodium cacodylate (pH 6.2) as previously described (*17*). For the anion-free complex, a crystal was cryoprotected by immersion for 2 s in 7% glycerol and then cryocooled by immersion in liquid nitrogen. The fluoride-soaked crystal was immersed for 2 min in reservoir solution to which 200 mM KF had been added and then cryoprotected and frozen. The azide complex crystal was immersed for 3 min in reservoir solution to which 25 mM sodium azide had been added, prior to cryoprotection and freezing. Diffraction data for the anion-free crystal were collected on beamline 24ID of the Argonne Synchrotron, while data for the other two crystals were collected on a rotating anode R-axis IV diffractometer. The anion-free structure was determined by molecular replacement as described previously (*17*). Diffraction data sets to resolutions of 1.7, 1.9, and 1.8 Å were collected for the three structures, 3CNQ, 3CO0, and 3BGO, respectively. Refinements of all three structures using REFMAC5 (*30*) and XFIT (*31*) led to R_{free} values of 0.23, 0.29, and 0.26, respectively. For each of the three structures, a difference map showing the scissile and C-terminal tail regions of the substrate, as well as the side chain of His 64 and the contents of the anion-binding pocket, was calculated before these components had been added to the structure, but after the remainder of the structure had been refined. These key components were thus built into unbiased maps. The molecular graphics program Coot (*32*) was used to superpose the three structures. Coordinates and complete statistics are available from the RCSB Protein Data Bank as entries 3CNQ (anion-free), 3CO0 (fluoride-soaked), and 3BGO (azide-bound).

RESULTS

The kinetics of pS169 activity as a function of azide concentration, measured in 0.1 M KPO$_4$ (pH 7.2), are shown in Figure 2.

Scheme 1

$$ES + anion \underset{\longleftarrow}{\overset{K_D}{\longrightarrow}} ES\text{-}anion \overset{k_2}{\longrightarrow} EP_1 + P_2$$

Because the complex of pS169 and substrate is very tight (the dissociation constant for the ES complex is <1 nM) and is preformed in the kinetic experiment, the data can be fit to a simple two-step mechanism:where E is pS169, S is pG12, P_1 consists of residues 1−77 of pG12, and P_2 is the released G_B domain. The apparent K_D for azide is 50 mM. The scissile bond cleavage which releases the G_B domain is concomitant with the acylation step in the enzymatic pathway. Because the complex of pS169 and P_1 is also very tight (the dissociation constant for the EP_1 complex is <1 nM), only one catalytic cycle is observed in this reaction. With no azide present, the rate of G_B release is 0.0019 s^{-1} at 22 °C. The rate of release in 100 mM azide is 4.1 s^{-1} at 22 °C, and the maximum rate in saturating azide (k_2) is 6.4 s^{-1} at 22 °C, corresponding to an azide-dependent rate enhancement of ~3300-fold. The anion-activated cleavage rate is on the same order as for the corresponding wild-type active site (Asp 32 version) of pS169, for which the rate of the acylation step is ~20 s^{-1} (data not shown).

Triggering by cyanate, formate, fluoride, and chloride was also examined for at least three concentrations of each anion. The apparent K_D values and the rates of cleavage at saturation for each are given in Table 1. Cyanate (pK_a = 3.46) is isosteric with azide (pK_a = 4.72) but binds more weakly and triggers more weakly at saturation. Formate (pK_a = 3.72) is a weaker trigger than cyanate. [We note that acetate (pK_a = 4.76) exhibits no detectable triggering activity presumably because it is too large to fit into the anion binding site.] Fluoride (pK_a = 3.16) strongly triggers pS169 (maximum rate of 11.2 s^{-1} in saturating fluoride) but with a K_D that is ~15-fold higher (apparent K_D of 0.75 M) than that of azide. Chloride (pK_a = −9) binds with an apparent K_D of >1 M and has a maximum rate of ~0.15 s^{-1} in saturating chloride. The ability of a particular anion to trigger proteolysis appears to be a complicated function of its size, shape, pK_a, and ability to accept a H-bond from His 64. For example, a non-hydrogen bonding anion such as chloride binds to the enzyme substrate complex but is a poor trigger. In contrast, a good H-bonding anion, such as fluoride, binds with an affinity similar to that of chloride but triggers ~100-fold faster. Inhibition of azide triggering by chloride was analyzed by measuring cleavage rates as a function of azide in 0.25 M KCl and in 0.5 M KCl. An apparent K_D of 1.2 M was calculated for chloride from the inhibition data, using a K_D of 50 mM for azide (in the absence of chloride) and a maximum rate of 6.4 s^{-1} in saturating azide.

The structures of the three pS164−substrate complexes with azide (3BGO), with fluoride (3CO0), and without added anions (3CNQ) are generally similar. Although the fluoride anion is a strong activator of the enzyme, its electron density is not distinguishable from water at this resolution, preventing identification of a fluoride binding site. In contrast, azide has a unique structure, and its location in the electron density map is clear. Unless otherwise specified, the following descriptions apply to the azide complex structure. Figure 3 shows the electron density for the azide anion, the His 64 side chain, and the scissile region of the substrate. The anion site is buried under the substrate, adjacent to the mutated Ala 32, 8 Å from the scissile peptide.

Table 1: Kinetic Parameters for Triggering Anions[a]

anion	pK_a	K_D (M)	k_2 (s^{-1})
azide	4.72	0.05	6.4
formate	3.72	0.6	1.2
cyanate	3.46	0.3	2.7
fluoride	3.16	0.75	11.2
chloride	−9.0	1.2	~0.15

[a]Rates were measured for at least three concentrations of each anion as described in Methods. K_D values and maximum rates at saturation were calculated according to Scheme 1 using Kintek Global Explorer.
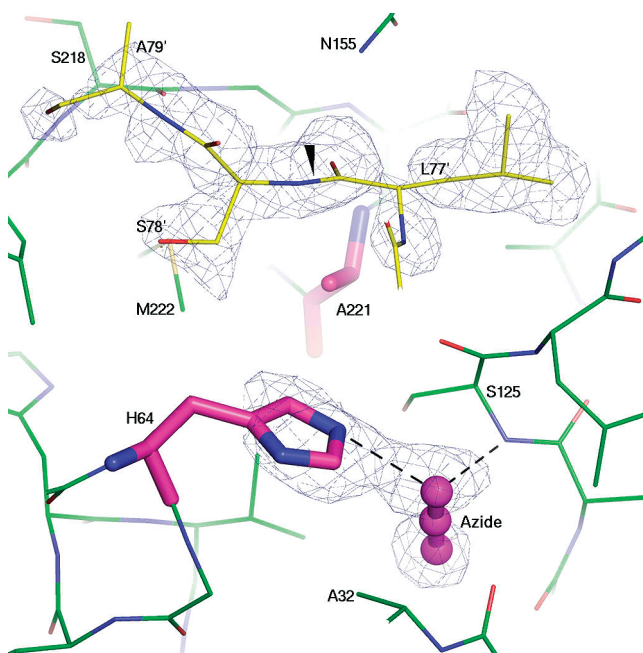

FIGURE 3: Unbiased electron density map showing the azide anion, the His 64 imidazole, and the scissile bond region of the substrate. The difference map is contoured at 2.5σ and shows the positions of all atoms in Ser 78′, and most atoms of Ala 79′. At lower contour values, the map is less clean but includes all atoms of residue 79′. A black triangle marks the scissile peptide. The two H-bonds from azide are both between 2.9 and 3.0 Å in length. The dumbbell-shaped electron density for azide is consistent with resonance theory that gives excess negative charge to its two terminal atoms.

Figure 4 shows the substrate bound across the active site. Both Ser 78′ (the prime symbol denotes the substrate) and Ala 79′ are in the β conformation, and Ala 79′ forms two H-bonds with Ser 218 of the enzyme, in a standard antiparallel β-sheet interaction. The side chain of Ser 78′ appears in two different conformations, depending on the presence of anion. In the anion-free structure, the conformation is the χ_1 = −60° rotamer, while in both the fluoride- and azide-soaked structures, the χ_1 torsion shifts to the 180° rotamer.

The dramatic stimulation of enzyme activity by azide and fluoride restores activity in otherwise marginally active D32A variants to near wild-type levels, suggesting that these anions functionally replace the Asp 32 carboxylate. In the generally accepted "catalytic triad" mechanism of wild-type subtilisin, the role of the Asp 32 carboxylate is to polarize the His 64 imidazole so that it removes the proton from the OG atom of Ser 221 and thus primes the OG atom for nucleophilic attack on the carbonyl carbon atom of the substrate's P1 residue (e.g., see ref *33* for a useful review). The D32A mutation was expected to create a small void adjacent to His 64, and we hypothesized that azide
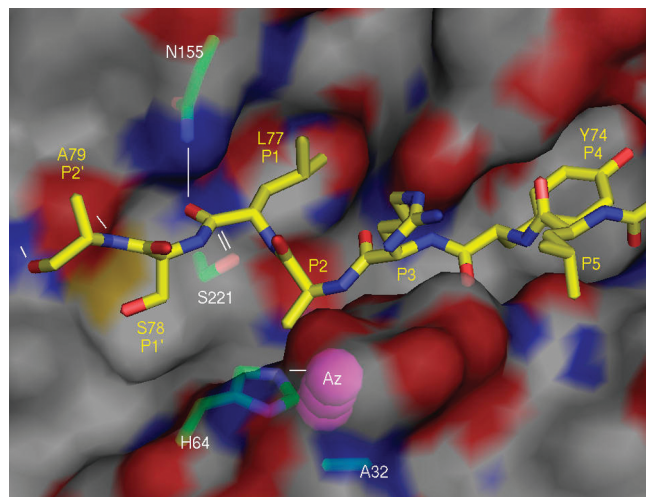
FIGURE 4: Structure of the substrate spanning the active site, in the azide complex. For the region shown, the substrate conformation is similar in all three structures, except for the Ser 78 side chain torsion and residue 79. The catalytic triad (Ala 221, His 64, and Ala 32), the oxyanion ligand Asn 155, and the azide anion are indicated. The position of the catalytic nucleophile 221 OG atom has been modeled, based on the wild-type structure (PDB entry 1CSE). White lines represent selected interactions < 3.3 Å in length. This image was created with Pymol and Image Magik.

would functionally replace the deleted carboxylate by binding in or near this void.

DISCUSSION

To model the mechanism of the active (Ser 221) form of the anion-triggered protease, we utilized the wild-type subtilisin structure 1CSE to model the position of the Ser 221 OG atom (*9*, *10*). Figure 5 shows the active site in the 3BGO azide complex, superimposed onto the wild-type active site of PDB entry 1CSE. Azide does not occupy the same location as the missing Asp 32 carboxylate (this would be prevented by steric overlap with the methyl group of Ala 32) but is in van der Waals contact with the methyl group (distance of 3.29 Å). The N_3 anion occupies a location that in many subtilisin structures accommodates a highly ordered water (at the location of the lower end of the azide) and often a second water (at the upper end of azide, the end nearest to His 64). The azide is within H-bonding distance of several nearby polar groups, including a 2.95 Å H-bond to the NE2 atom of His 64. The conformation of His 64 in 3BGO stands in comparison with the canonical active rotamer for His 64 as observed in 1CSE, where $\chi_1 = -180°$ and the imidazole forms H-bonds both to Asp 32 and to Ser 221. In 3BGO, the His 64 $\chi_1 = 124°$, placing the imidazole 4.16 Å from Ala 221. This conformation is torsionally unfavorable but minimizes the distance to the azide anion, suggesting that the interaction with azide is the primary force setting the position of the His 64 imidazole.

In the wild-type active site of the 1CSE structure, all three interactions along the "charge-relay" chain (Asp 32−His 64−Ser 221−substrate) are shorter than 3 Å, and thus, it appears that electronic and H-ion motions alone can trigger the nucleophilic attack that initiates proteolysis. In contrast, in all three of these structures (anion-free, with fluoride, and with azide), the His 64 rotamer is swung somewhat away from Ala 221 and toward Ala 32 (shortest distance from imidazole ring to the modeled Ser 221 OG atom is 4.2 Å). This torsional excursion is made possible by removing the Asp 32 side chain, which opens the space into which
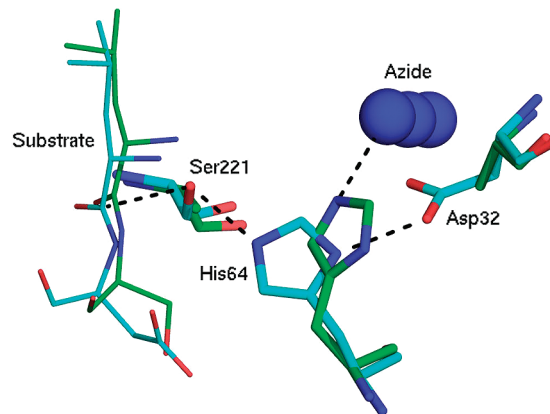

FIGURE 5: Superposition of the catalytic triad in the eglin complex (1CSE, cyan) onto the corresponding residues in the azide complex (3BGO, green). In the 1CSE structure, the three dashed lines (the three not involving azide) connecting substrate, Ser 221, His 64, and Asp 32 are all < 3 Å in length. In the azide complex, the 2.9 Å H-bond between His 64 and azide is shown.

the imidazole swings. Another factor governing His 64's position appears to be a steric "push" from the substrate's P1′ side chain (Ser 78′), which is 4.1 Å from His 64 (Cβ−Cβ distance) (*34*). The P1′ side chain sterically blocks the His 64 imidazole from adopting the outward $\chi_1 = -60°$ rotamer, constraining it toward its observed position where it is adjacent to Ala 32 and adjacent to the anion site. When substrate is omitted, His 64 is observed with χ_1 in the $-60°$ rotamer, pointing away from Ala 32 and placing the imidazole ring well away from contact with either Ala 32 or Ala 221. This has been observed in the substrate-free D32A active site in PDB entry 3F49. It thus appears that the P1′ residue of the substrate helps to position His 64 for catalysis in D32A variants. Accordingly, once His 64 is pushed approximately into the active χ_1 conformation by substrate binding, the imidazole's ability to ionize makes the adjacent cavity favorable for binding anions. This is consistent with the inability of azide or fluoride to accelerate the cleavage rate of peptide substrates with *p*-nitroanilide or amino methyl coumarin leaving groups (*21*), which suggests that productive anion binding requires the presence of a P1′ amino acid.

Since the Ser 221 form of these structures is activated by anions, evidently His 64 is able to swing back toward Ser 221 sufficiently to accept its proton and thus stimulate its nucleophilic attack on the substrate. This is also consistent with the fact that, in all three of these structures, but especially in the two anion-bound structures, the electron density for the His 64 side chain is observed to be slightly smeared over a range of torsions. The angular extent of its local disorder appears to be ~50−70°. This suggests that His 64 swings across a range of χ_1 positions and transiently occupies an active position with a sufficient frequency to enable efficient proteolysis. Although the protonation state of His 64 is not known, and the observed torsional disorder could be associated with an oscillating protonation state, the imidazole must be deprotonated to be active; hence, we will focus on the mechanistic role of the deprotonated state. One additional uncertainty is generated by the unknown χ_2 rotameric state of the imidazole (ring flip). While in the eglin structure the positions of the ring nitrogens are clearly inferred from the H-bonding interactions, in the azide complex the observed H-bond between azide and His 64 is consistent with either χ_2 rotamer.

The observed position of azide is not compatible, for any static His 64 rotamer, with a simple, fixed-atom proton shuttle as in

1CSE. If azide remains in the observed site, the His 64 side chain must play a dynamic, mobile role to fulfill its expected charge-relay function, interacting with both anion and Ser 221. Alternatively, it is possible that, in addition to the imidazole repositioning so as to H-bond to Ser 221, the azide (or other anion) also moves from the observed site, a distance of $\sim$2 Å, to occupy a more Asp 32-like position compatible with a static charge-relay triad as in the wild type. This last possibility is most economical, in spite of the fact that it requires a small steric shift from the observed structure, because it preserves the fundamental roles and interactions of the wild-type mechanism, simply replacing the Asp 32 carboxylate with the triggering anion. In this model, some motion of the His 64 imidazole appears to be required for its effective interaction with Ser 221, but the precise dynamics of His 64 remain unresolved.

ACKNOWLEDGMENT

REFERENCES

1. Ottesen, M., and Svendsen, I. (1970) The Subtilisins. *Methods Enzymol. 19*, 199–215.
2. Wells, J. A., Ferrari, E., Henner, D. J., Estell, D. A., and Chen, E. Y. (1983) Cloning, sequencing and secretion of *Bacillus amyloliquifaciens* subtilisin in *Bacillus subtilis*. *Nucleic Acids Res. 11*, 7911–7925.
3. Vasantha, N., Thompson, L. D., Rhodes, C., Banner, C., Nagle, J., and Filpula, D. (1984) Genes for alkaline and neutral protease from *Bacillus amyloliquifaciens* contain a large open-reading frame between the regions coding for signal sequence and mature protein. *J. Bacteriol. 159*, 811–819.
4. Khan, A. R., and James, M. N. (1998) Molecular mechanisms for the conversion of zymogens to active proteolytic enzymes. *Protein Sci. 7*, 815–836.
5. Power, S. D., Adams, R. M., and Wells, J. A. (1986) Secretion and autoproteolytic maturation of subtilisin. *Proc. Natl. Acad. Sci. U.S.A. 83*, 3096–3100.
6. Ikemura, H., Takagi, H., and Inouye, M. (1987) Requirement of pro-sequence for the production of active subtilisin E in *Escherichia coli*. *J. Biol. Chem. 262*, 7859–7864.
7. Gallagher, T. D., Gilliland, G., Wang, L., and Bryan, P. (1995) The prosegment-subtilisin BPN' complex: Crystal structure of a specific foldase. *Structure 3*, 907–914.
8. Berger, A., and Schechter, I. (1970) Mapping the active site of papain with the aid of peptide substrates and inhibitors. *Philos. Trans. R. Soc. London, Ser. B 257*, 249–264.
9. McPhalen, C. A., Schnebli, H. P., and James, M. N. (1985) Crystal and molecular structure of the inhibitor eglin from leeches in complex with subtilisin Carlsberg. *FEBS Lett. 188*, 55–58.
10. Bode, W., Papamokos, E., Musil, D., Seemueller, U., and Fritz, H. (1986) Refined 1.2 Å crystal structure of the complex formed between subtilisin Carlsberg and the inhibitor eglin c. Molecular structure of eglin and its detailed interaction with subtilisin. *EMBO J. 5*, 813–818.
11. Bryan, P., Alexander, P., Strausberg, S., Schwarz, F., Lan, W., Gilliland, G., and Gallagher, D. T. (1992) Energetics of folding subtilisin BPN'. *Biochemistry 31*, 4937–4945.
12. Gallagher, T., Bryan, P., and Gilliland, G. L. (1993) Calcium-independent subtilisin by design. *Proteins 16*, 205–213.
13. Bech, L. M., Sorensen, S. B., and Breddam, K. (1992) Mutational replacements in subtilisin 309. Val104 has a modulating effect on the P4 substrate preference. *Eur. J. Biochem. 209*, 869–874.
14. Gron, H., and Breddam, K. (1992) Interdependency of the binding subsites in subtilisin. *Biochemistry 31*, 8967–8971.
15. Rheinnecker, M., Eder, J., Pandey, P. S., and Fersht, A. R. (1994) Variants of subtilisin BPN' with altered specificity profiles. *Biochemistry 33*, 221–225.
16. Georgieva, D. N., Genov, N., and Betzel, C. (2005) *Bacillus licheniformis* variant DY proteinase: Specificity in relation to the geometry of the substrate recognition site. *Curr. Microbiol. 51*, 71–74.
17. Ruan, B., London, V., Fisher, K. E., Gallagher, D. T., and Bryan, P. N. (2008) Engineering Substrate Preference in Subtilisin: Structural and Kinetic Analysis of a Specificity Mutant. *Biochemistry 47*, 6628–6636.
18. Ruvinov, S., Wang, L., Ruan, B., Almog, O., Gilliland, G. L., Eisenstein, E., and Bryan, P. N. (1997) Engineering the independent folding of the subtilisin BPN' prodomain: Analysis of two-state folding versus protein stability. *Biochemistry 36*, 10414–10421.
19. Ruan, B., Hoskins, J., Wang, L., and Bryan, P. N. (1998) Stabilizing the subtilisin BPN' pro-domain by phage display selection: How restrictive is the amino acid code for maximum protein stability? *Protein Sci. 7*, 2345–2353.
20. Craik, C. S., Roczniak, S., Largman, C., and Rutter, W. J. (1987) The catalytic role of the active site aspartic acid in serine proteases. *Science 237*, 909–913.
21. Ruan, B., Fisher, K. E., Alexander, P. A., Doroshko, V., and Bryan, P. N. (2004) Engineering subtilisin into a fluoride-triggered processing protease useful for one-step protein purification. *Biochemistry 43*, 14539–14546.
22. Takahashi, E., and Wraight, C. A. (2006) Small weak acids reactivate proton transfer in reaction centers from *Rhodobacter sphaeroides* mutated at AspL210 and AspM17. *J. Biol. Chem. 281*, 4413–4422.
23. Strausberg, S. L., Alexander, P. A., Gallagher, D. T., Gilliland, G. L., Barnett, B. L., and Bryan, P. N. (1995) Directed evolution of a subtilisin with calcium-independent stability. *Nat. Biotechnol. 13*, 669–673.
24. Alexander, P. A., Ruan, B., Strausberg, S. L., and Bryan, P. N. (2001) Stabilizing mutations and calcium-dependent stability of subtilisin. *Biochemistry 40*, 10640–10644.
25. Almog, O., Gallagher, D. T., Ladner, J. E., Strausberg, S., Alexander, P., Bryan, P., and Gilliland, G. L. (2002) Structural basis of thermostability. Analysis of stabilizing mutations in subtilisin BPN'. *J. Biol. Chem. 277*, 27553–27558.
26. Strausberg, S. L., Ruan, B., Fisher, K. E., Alexander, P. A., and Bryan, P. N. (2005) Directed coevolution of stability and catalytic activity in calcium-free subtilisin. *Biochemistry 44*, 3272–3279.
27. Alexander, P., Fahnestock, S., Lee, T., Orban, J., and Bryan, P. (1992) Thermodynamic analysis of the folding of the streptococcal protein G IgG-binding domains B1 and B2: Why small proteins tend to have high denaturation temperatures. *Biochemistry 31*, 3597–3603.
28. Alexander, P. A., He, Y., Chen, Y., Orban, J., and Bryan, P. N. (2007) The design and characterization of two proteins with 88% sequence identity but different structure and function. *Proc. Natl. Acad. Sci. U.S.A. 104*, 11963–11968.
29. Bryan, P. N. (1995) Subtilisin Engineered for facile folding: Analysis of uncatalyzed and prodomain-catalyzed folding. In Intramolecular chaperones and protein folding (Shinde, U., and Inouye, M., Eds.) pp 85−112, R. G. Landes, Austin, TX.
30. Murshudov, G. N., Vagin, A. A., and Dodson, E. J. (1997) Refinement of macromolecular structures by the maximum-likelihood method. *Acta Crystallogr. D53*, 240–255.
31. McRee, D. E. (1999) XtalView/Xfit: A versatile program for manipulating atomic coordinates and electron density. *J. Struct. Biol. 125*, 156–165.
32. Emsley, P., and Cowtan, K. (2004) Coot: Model-building tools for molecular graphics. *Acta Crystallogr. D60*, 2126–2132.
33. Hedstrom, L. (2002) Serine protease mechanism and specificity. *Chem. Rev. 102*, 4501–4524.
34. Radisky, E. S., Kwan, G., Karen Lu, C. J., and Koshland, D. E., Jr. (2004) Binding, Proteolytic, and Crystallographic Analyses of Mutations at the Protease-Inhibitor Interface of the Subtilisin BPN'/Chymotrypsin Inhibitor 2 Complex. *Biochemistry 43*, 13648–13656.